Primostrato Solid-State NMR Enhanced by Dynamic Nuclear Polarization: Pentacoordinated Al 3+ Ions Are Only Located at the Surface of Hydrated γ-Alumina

Daniel Lee, Nghia Tuan Tuan Duong, Olivier Lafon, Gaël de Paëpe

Primostrato Solid-State NMR Enhanced by Dynamic Nuclear Polarization: Penta-Coordinated Al^{3+} are Only Located at the Surface of Hydrated γ-Alumina

Daniel Lee[†,§], *Nghia Tuan Duong*[†,§,‡], *Olivier Lafon*[‡] *and Gaël De Paëpe**[†,§]

[†] Univ. Grenoble Alpes, INAC, SCIB, F-38000 Grenoble, France.

[§] CEA, INAC, SCIB, F-38000 Grenoble, France.

[‡] Univ. Lille Nord de France; CNRS UMR 8181, Unité de Catalyse et de Chimie du Solide (UCCS), Univ. Lille 1, 59652 Villeneuve d'Ascq Cedex, France.

ABSTRACT

Aluminas (Al_2O_3) are ubiquitous functional materials. In particular, the γ-alumina form is extensively used in research and industry as a catalyst and catalyst support. Nevertheless, a full structural description, which would aid comprehension of its properties, is lacking and under large debate. Solid-state NMR has been used previously to study γ-alumina but is limited for

certain applications, such as surface studies, due to intrinsic low sensitivity. Here, we detail the implementation of low temperature (~100 K) magic angle spinning combined with dynamic nuclear polarization (MAS-DNP) to significantly enhance the sensitivity of solid-state NMR experiments and gain structural insights into this important material. Notably, we analyze hydrophilic and hydrophobic sample preparation protocols and their implications on the sample and resulting NMR parameters. We show that the choice of preparation does not perturb the spectrum, but it does have a large effect on NMR coherence lifetimes, as does the corresponding required (hyper-)polarizing agent. We use this preliminary study to optimize the absolute sensitivity of the following experiments. We then show that there are no detectable hydroxyl groups in the bulk of the material and that DNP-enhanced $^{1}H \rightarrow {}^{27}Al$ cross-polarization experiments are selective to only the first surface layer, enabling a very specific study. This *primostrato* NMR is integrated with MQMAS and it is demonstrated, interestingly, that penta-coordinated Al^{3+} ions are only observed in this first surface layer. To highlight that there is no evidence of sub-surface penta-coordinated Al^{3+}, a new *bulk-filtered* experiment is described that can eliminate surface signals.

KEYWORDS: DNP, solid-state NMR, homonuclear correlation, MQMAS, alumina, penta-coordinated aluminum

1. INTRODUCTION

A variety of techniques are available for the characterization of surfaces (ion beam analysis, electron spectroscopy, proximal probes, X-ray techniques, optical techniques, scanning-tunneling microscopy etc.).[1] As always, each technique will exhibit specific benefits but will also suffer

from specific limitations (e.g. limit of detection, spatial and time resolution, penetration depth, restrictions on sample type, cost and availability…). So far, Solid-State Nuclear Magnetic Resonance (SSNMR) spectroscopy has been largely overlooked by the surface characterization community. This is possibly due to the major specific limitation of NMR: its low intrinsic sensitivity. This deterrent is accentuated when considering surfaces, which usually constitute only a small fraction of the studied sample. However, following founding work by Griffin and co-workers in the successful combination of high-field SSNMR under Magic Angle Spinning with Dynamic Nuclear Polarization (MAS-DNP),[2] surfaces have been increasingly studied by this technique.[3]

DNP involves the transfer of the substantial spin-polarization of unpaired electrons to nearby nuclei driven by microwave (μw) irradiation near the Electron Paramagnetic Resonance (EPR) frequency. By this approach the net polarization of the nuclei is greatly enhanced. Since the extent of polarization relates directly to the observable NMR signal, the use of DNP results in spectra with greatly enhanced signal-to-noise (S/N) ratios, reducing required experimental times and allowing for fast characterization of surfaces.

NMR can selectively explore surfaces when there is a difference to the bulk that can be exploited. For surfaces that are protonated (compared to a non-protonated bulk), Cross Polarization (CP)[4] from protons to the nuclei of interest then results in excitation of only near surface nuclei. This was demonstrated in the early 1980s by Maciel and Sindorf for $^{1}H \rightarrow ^{29}Si$ CP in silicon dioxide (SiO_2) type materials[5] and also in the late 1980s for $^{1}H \rightarrow ^{27}Al$ CP in aluminas (Al_2O_3) by Morris and Ellis.[6] The latter could be deemed highly impressive, since it involves polarization transfer to a quadrupolar isotope, ^{27}Al.

Quadrupolar nuclei (nuclei with spin > ½) account for the considerable majority of NMR-active nuclei (74 %), including many technologically and biologically important isoptopes (^{6,7}Li, ^{14}N, ^{17}O, ^{23}Na, ^{27}Al etc.), and, unfortunately, conventional SSNMR radio-frequency (RF) irradiation sequences can return very low efficiencies due to the intricate spin dynamics of these nuclei in the presence of RF fields and MAS. Furthermore, the situation is compounded by the spectral broadening resulting from the residual quadrupolar interaction that cannot be completely removed by MAS. This broadening further reduces the obtainable S/N, often to undetectable limits.[7] Even though SSNMR spectroscopy presents itself as a technique that is able to provide detail on the atomic-level structure of even heterogeneous and disordered systems, the intrinsic insensitivity and the problems described above present a particular obstacle when knowledge of the local environment of quadrupolar nuclei is desired.

This is the case for the oxide of aluminium, alumina (Al_2O_3), which contains the spin-5/2 nucleus ^{27}Al at 100% natural isotopic abundance. Alumina exists under several crystal forms. In particular, γ-alumina is widely-used in industry as catalyst supports and as a catalyst owing to the combination of favorable textural properties (high surface area of about 300 $m^2.g^{-1}$)[8] and its Lewis/Brønsted-Lowry acid/base characteristics.[9] For instance, γ-alumina is used as a catalyst support in a variety of industrial processes, such as the production of butadiene used in synthetic rubber, desulfurization and automobile exhaust gas catalytic converters.[10] Single-site catalysts supported on γ-alumina are also highly-active for various reactions, such as alkene polymerization and metathesis.[11,12] γ-alumina is also used as a catalyst in important industrial processes, such as alcohol dehydration and the Claus process, which is used to recover sulphur from hydrogen sulphide. Another major application of γ-alumina is its use as an absorbent for various applications, such as gas or liquid drying as well as water purification.[9]

However, in spite of the large interest and use of γ-alumina, its structure is still under heavy investigation since it does not yield single crystals suitable for standard structural analysis using diffraction techniques. Most γ-alumina samples consist of nanoparticles with a size of ~10-30 nm containing an inner crystalline core.[8] The bulk of γ-alumina contains both hexa- (Al^{VI}) and tetra- (Al^{IV}) coordinated alumina sites, the former being more abundant than the latter.[13–15] It has been suggested that the structure of the bulk exhibits many defects, including the presence of penta-coordinated (Al^{V}) sites, variation in cation occupancies and related distorsions of tetra- and octa-hedral Al environments. γ-alumina also exhibits a large variety of surface sites. The nature of the sites depends on the termination crystallographic plane as well as the hydration of the surface, which can be controlled by thermal treatment.[7] Surface models have been proposed based on infrared spectroscopy,[16] ^{1}H and ^{27}Al solid-state NMR spectroscopy[6,17–22] as well as Density-Functional Theory (DFT) calculations.[13,23] Some of the surface Al atoms are bonded to hydroxyl groups or water molecules. The hydroxyl groups can be terminal (linked to a single Al atom) as well as doubly and triply bridging. The surface of γ-alumina is also covered by physisorbed water in the absence of thermal treatment.

In this work it is shown that SSNMR can be used to selectively probe both the surface and the bulk of commercially available γ-alumina nanoparticles. Significantly, it is demonstrated that the surface selection is limited to the first surface layer of the material, yielding *primostrato* NMR. For the specific selection of bulk material a new experiment is detailed. The inclusion of DNP to enhance the S/N of the *primostrato* SSNMR experiments was required to alleviate the associated sensitivity problems. Moreover, it is also shown that the environment used for MAS-DNP experiments (low temperatures, paramagnetic polarizing agents, solvents) can affect the nuclear relaxation times, although the ^{27}Al NMR lineshapes remain unchanged, suggesting that the

sample's structure is not perturbed. Owing to a time-saving factor ~90 obtained for DNP-enhanced experiments compared to room temperature experiments, Multiple Quantum Magic Angle Spinning (MQMAS)[24,25] and ^{27}Al homonuclear dipolar-mediated correlation two-dimensional (2D) experiments could be acquired for the surface of γ-alumina in reasonable time (< 7 hours). The former is used to obtain a high-resolution spectral dimension to better distinguish Al sites and obtain quadrupolar-coupling parameters, whereas the latter is used to resolve relative spatial proximities between the various Al sites. The selectivity of these experiments allows information to be attained that shows that a small amount of Al^V sites are present in hydroxylated environments in the first surface layer of the hydrated γ-alumina, whereas Al^V sites in the bulk are not detected.

2. EXPERIMENTAL METHODS

The γ-alumina nanopowder was purchased from Sigma-Aldrich and used as received. This nanopowder was placed directly into a 3.2 mm thin-walled zirconia rotor for both room temperature and low temperature (~ 100 K) SSNMR measurements on the pure sample. For the 'DNP ready' samples, 30 mg of the nanopowder was mixed gently with a 40 μL aliquot of the chosen 'DNP matrix'. A known mass (usually 60-100 mg) of the resulting wet powder was placed into the (previously emptied) 3.2 mm rotor; the same rotor was used for all the experiments. The mass of the γ-alumina itself inside the rotor was calculated so that returned NMR signal could be compared between experiments. For a hydrophobic sample preparation, the 'DNP matrix' was the *bis*-TEMPO-*bis*-Ketal (bTbK) biradical polarizing agent dissolved in 1,1,2,2-tetrabromoethane (TBE).[26] For an aqueous sample preparation, the 'DNP matrix' was the 1-(TEMPO-4-oxy)-3-(TEMPO-4-amino)propan-2-ol (TOTAPOL) biradical polarizing agent[27]

dissolved in a mixture of perdeuterated dimethylsulfoxide ([$^2H_6$]DMSO), deuterated water (^2H_2O) and pure water (H_2O) (78, 14, 8 wt %, respectively). For a comparison of the two polarizing agents used here, a matrix was also prepared where bTbK was dissolved in the same [$^2H_6$]DMSO/^2H_2O/H_2O mixture. The TBE and ^2H_2O were purchased from Sigma-Aldrich and the [$^2H_6$]DMSO from VWR. All were used without further purification. The TOTAPOL biradical was synthesized following the published procedure[27] and Prof. Paul Tordo and Dr Olivier Ouari from the Université d'Aix-Marseille donated the bTbK biradical.

The conventional SSNMR experiments were performed on a Bruker AVANCE 400 MHz (9.4 T) spectrometer operating at 298 K using a Bruker 3.2 mm triple-resonance MAS probe. The low temperature and DNP experiments were performed on a Bruker DNP-SSNMR AVANCE III 400 MHz spectrometer equipped with a gyrotron and transmission line capable of providing ~5 W of 263 GHz μw irradiation at the sample and a low-temperature 3.2 mm MAS probe suitable for spinning rates of up to ~15 kHz and sample temperatures of ~100 K.[28] For further experimental details, including calibration of efficient CP to half-integer-spin quadrupolar ^{27}Al nuclei, see the Supporting Information.

3. RESULTS AND DISCUSSION

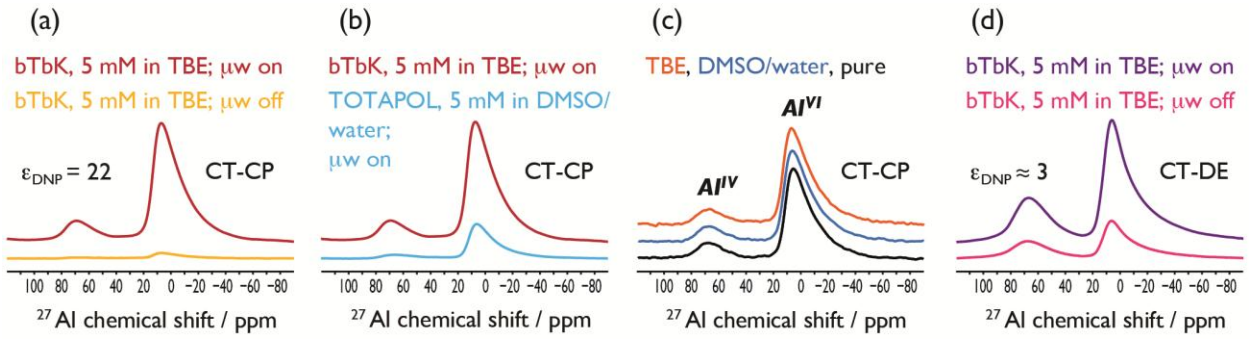

Figure 1. ^{27}Al NMR spectra recorded with a MAS rate of ~14 kHz and a sample temperature of ~104 K. (a) ^{1}H→^{27}Al CT-CP spectra of γ-alumina impregnated with 5 mM bTbK in TBE illustrating the indirect DNP enhancement. (b) The top spectrum from (a) compared with the ^{1}H→^{27}Al CT-CP spectrum of γ-alumina impregnated with 5 mM TOTAPOL in [$^{2}H_6$]DMSO/$^{2}H_2O$/H_2O (labelled as DMSO/water in the figure). The intensity of the spectra in (b) is proportional to the ASR. (c) ^{1}H→^{27}Al CT-CP spectra of pure γ-alumina and γ-alumina impregnated with TBE or [$^{2}H_6$]DMSO/$^{2}H_2O$/H_2O mixture. (d) ^{27}Al CT-DE spectra of γ-alumina impregnated with 5 mM bTbK in TBE illustrating the direct DNP enhancement.

The signal enhancement as a result of the DNP can be clearly seen in Fig. 1 (a). Continuous μw irradiation is applied at a frequency suitable to drive DNP from unpaired electrons of the bTbK biradical polarizing agent to solvent or sample ^{1}H nuclei, using the Cross-Effect (CE) under MAS polarization transfer process.[29,30] These hyperpolarized ^{1}H nuclei are then used to transfer their polarization to interfacial/surface ^{27}Al nuclei of the γ-alumina via a Central-Transition Cross-Polarization (CT-CP) experiment.[31] The time constant for polarization build-up was identical with and without μw irradiation, as already observed for other systems, when using biradical polarizing agents.[32] A comparison of the returned signal intensity between experiments acquired with identical recycle delay with and without continuous μw irradiation gives the signal enhancement, ε_{DNP}, as a result of the hyperpolarization process. For the experimental conditions used to record the spectra of Fig. 1 (a), $\varepsilon_{DNP} = 22$.

ε_{DNP} is an important number as it illustrates how effectively the hyperpolarization process is working. Nonetheless, we have recently demonstrated that this value alone is not sufficient to determine whether the DNP experiment is more worthwhile than conventional NMR.[33]

Recording MAS NMR spectra under contemporary conditions used for DNP brings sensitivity enhancements (e.g. ε_{DNP}) but also sensitivity reductions for various reasons (sample dilution, paramagnetic bleaching…) which we have detailed elsewhere.[33] To this extent we introduced the Absolute Sensitivity Ratio (ASR), which is a ratio of the signal-to-noise per unit square root of time between an experiment recorded under DNP conditions and under conventional SSNMR conditions. The ASR is then a direct measure of the relevance of performing DNP. For instance, Fig. 1 (b) shows two DNP-enhanced $^{1}H\rightarrow^{27}Al$ CT-CP spectra of γ-alumina recorded using different sample preparation methods. These spectra have been scaled to conform to the ASR (i.e., the relative S/N for the same experimental time). The ASR shows that impregnation of γ-alumina with 5 mM bTbk solution in TBE results in higher NMR sensitivity than an impregnation with 5 mM TOTAPOL solution in $[^{2}H_6]DMSO/^{2}H_2O/H_2O$. A further analysis on possible sample preparations and corresponding ASRs is given below.

One question about the applicability of DNP concerns the effects of adding solvents and polarizing agents to the sample of interest. Indeed, in a recent study of γ-alumina using DNP-enhanced SSNMR it was stated that the addition of H_2O and/or the TOTAPOL biradical polarizing agent led to the absence of penta-coordinated Al^{3+}.[34] The relevance of adding various substances to the sample of interest depends on the conditions that one wants to study. For example, γ-alumina can be useful in aqueous,[35] hydrophobic,[36] and also dry conditions.[12,37] Since $^{1}H\rightarrow^{27}Al$ CT-CP spectra of γ-alumina only display the signal of surface ^{27}Al nuclei,[6] the comparison of $^{1}H\rightarrow^{27}Al$ CT-CP spectra of γ-alumina shown in Fig. 1 (c) demonstrate that the surface does not undergo significant changes, in terms of the ratios of Al^{IV} and Al^{VI} coordination states and quadrupolar parameters, upon the addition of either a mixture of DMSO and water or hydrophobic TBE, compared to the pure nanopowder. The sample of γ-alumina was used as

received, without any calcination pretreatment. Therefore, the sample was likely to have been in a fully hydrated state, for which the surfaces of the nanoparticles are fully covered by chemi- and physi-sorbed water molecules. Hence, the addition of the solvents would then not have any effect on the surface coordination. Note that an Al^{V} coordination state cannot be resolved in the one-dimensional (1D) spectra here but is investigated further below. Although the various sample conditions presented seem to have minimal effect on the ^{27}Al 1D NMR spectrum, they affect the measured decay times of NMR coherences; this is analyzed in detail below.

MAS-DNP is not only suitable for enhancing the polarization of protons but it can also be used to enhance the polarization of other nuclei directly, without the need for a CP step.[38–42] Fig. 1 (d) shows direct DNP enhancement ($\varepsilon_{DNP} = 3$) of the ^{27}Al nuclei of γ-alumina impregnated with 5 mM bTbK in TBE, using Central-Transition Direct-Excitation (CT-DE) experiments acquired with and without continuous μw irradiation. There is no difference in lineshape between these two spectra (see Fig. S1 (a)). Under similar conditions but using 5 mM TOTAPOL in $[^{2}H_6]DMSO/^{2}H_2O/H_2O$, the direct DNP enhancement was almost negligible: $\varepsilon_{DNP} \approx 1$ (see Fig. S1 (b)). Small direct enhancement ($\varepsilon_{DNP} = 3$) could be expected for many reasons. (i) The DNP frequency matching conditions used were optimized for protons and not adjusted accordingly for the direct enhancement of ^{27}Al. (ii) The polarizing agents used (bTbK and TOTAPOL) were designed for DNP of protons and other polarizing agents could be more suited for direct hyperpolarization of ^{27}Al nuclei.[41] (iii) Unlike the case for ^{1}H, the polarizing agents are not uniformly distributed around all the ^{27}Al nuclei because they are external to the nanoparticulate γ-alumina. Additionally, DNP-induced spin diffusion will be much slower in this case as compared to DNP of ^{1}H in substantially protonated particulate systems.[43] Thus, there will be a hyperpolarization gradient with the largest enhancement near the surface and the smallest

enhancement at the centre of the nanoparticle.[44] The overall enhancement, ε_{DNP}, will be an average and will depend upon the diameter of the nanoparticle and the hyperpolarization depth.[39,45] It then appears that Al^{VI} sites reside, on average, closer to the surface since they return a larger direct DNP enhancement than Al^{IV} sites (see Fig. S1 (a)). It is worth noting that this is taking into account a similar longitudinal relaxation and quadrupolar coupling for the two sites as dissimilarity could result in different efficiency of DNP. The possibility to perform direct DNP to ^{27}Al is interesting, for example for studies of dehydroxylated aluminas where indirect DNP, via protons, is not possible or for studies beyond the surface of the nanoparticle.[38] A full study of this direct DNP enhancement will be published elsewhere.

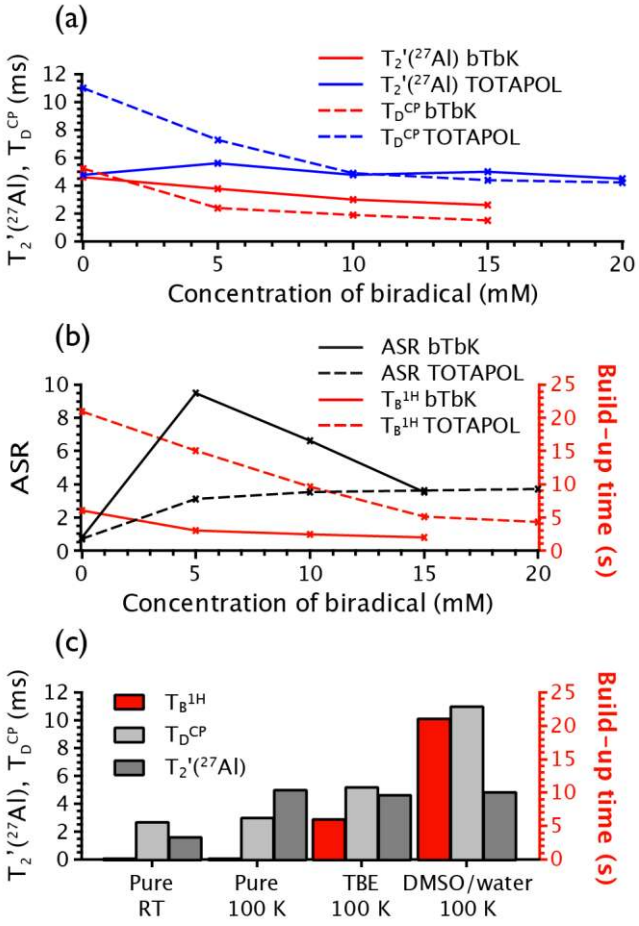

Figure 2. Dependence of NMR parameters for studies on γ-alumina with biradical concentration, type, and the solvent used. (a) Variation of $T_2'(^{27}Al)$ (solid lines) and T_D^{CP} (dashed lines) with TOTAPOL concentration in $[^2H_6]DMSO/^2H_2O/H_2O$ (blue) and with bTbK concentration in TBE (red). (b) Variation of the ^1H polarization build-up time constant, T_B^{1H}, (red) and the ASR (black) with TOTAPOL concentration in $[^2H_6]DMSO/^2H_2O/H_2O$ (dashed lines) and with bTbK concentration in TBE (solid lines). (c) Variation of $T_2'(^{27}Al)$ (dark grey), T_D^{CP} (light grey), and T_B^{1H} (red) for pure γ-alumina at room temperature, 104 K and at 104 K when mixed with TBE or $[^2H_6]DMSO/^2H_2O/H_2O$ in the absence of biradicals. All the data were recorded using an initial CT-CP step, with a MAS rate of ~ 14 kHz and at a sample temperature fixed at 104 K (unless specified otherwise). Connecting lines are used as guides only.

The change in various NMR parameters depending upon the sample condition is shown in Fig. 2. The time constant for the signal decay during a CT-CP step, labeled here T_D^{CP}, can be measured by varying the time for which this step is applied and fitting the resulting change in signal intensity to a combined build-up and decay of signal.[46] This empirical time constant, T_D^{CP}, cannot be assumed as a simple combination of $T_{1\rho}^{1H}$ and $T_{1\rho}^{27Al}$, the time constants for decay under spin-locking of ^1H and ^{27}Al nuclei involved in CP, respectively, owing to the different spin dynamics between CP and single-channel spin-locking. The variation of this decay as a function of biradical concentration for two different solvent/biradical combinations is given in Fig. 2 (a). The two combinations represent aqueous (TOTAPOL in $[^2H_6]DMSO/^2H_2O/H_2O$) and hydrophobic/organic (bTbK in TBE) sample preparation protocols that are commonplace for MAS-DNP experiments. As expected, for both combinations, an increase in the concentration of radicals around the γ-alumina sample leads to a faster decay of signal and thus shorter T_D^{CP}. What is interesting here is the effect of the different solvents. The aqueous solvent mixture leads

to intrinsically longer T_D^{CP} values compared to the organic solvent (in the absence of radical doping). Even at relatively high concentrations (10-20 mM) for TOTAPOL in aqueous solvent, the T_D^{CP} values are similar to γ-alumina in TBE alone. As soon as the concentration of bTbK is increased above 0 mM, the induced reduction of T_D^{CP} times is dramatic. Furthermore, when compared to pure (no solvent) γ-alumina at 104 K, there is a significant increase in T_D^{CP} upon the addition of radical-free frozen solvent, as shown in Fig. 2 (c). However, there is no significant change in T_D^{CP} between RT and 104 K for the pure γ-alumina. Therefore, the increased T_D^{CP} originates from the addition of frozen solvent and could result from markedly reduced ^{1}H dynamics and/or the removal of paramagnetic oxygen from the surface of the γ-alumina.

Another important time constant for signal decay during ^{27}Al NMR experiments is $T_2'(^{27}\text{Al})$. This is the time constant for the decay during a spin-echo block applied to ^{27}Al nuclei (with continuous application of sufficient ^{1}H heteronuclear decoupling). To be selective for the surface of γ-alumina, the $T_2'(^{27}\text{Al})$ values were measured after an initial CT-CP step. The variation of $T_2'(^{27}\text{Al})$ as function of biradical concentration at 104 K is given in Fig. 2 (a). As the concentration of TOTAPOL increases for the aqueous sample, there seems to be negligible effect on the $T_2'(^{27}\text{Al})$ value, except for experimental fluctuations. However, for the organic preparation, as the concentration of bTbK increases, $T_2'(^{27}\text{Al})$ steadily decreases (albeit modestly). Furthermore, in the absence of biradicals, the $T_2'(^{27}\text{Al})$ is similar for both the aqueous and organic solvent preparations and also the pure γ-alumina at 104 K (Fig. 2 (c)). This latter observation suggests that the solvent does not affect the $T_2'(^{27}\text{Al})$. However, unlike for the case of T_D^{CP}, it is clear from Fig. 2 (c) that temperature does have an effect on $T_2'(^{27}\text{Al})$ since the value is more than 3 times larger for the pure γ-alumina at 104 K compared to at RT. We have recently shown that the effect of increasing the TOTAPOL concentration from 0 to 20 mM on

the T_2' of the spin-1/2 ^{13}C nucleus of urea solution in an DMSO/water mixture was a decrease in T_2'(^{27}Al) from approximately 45 to 10 ms.[47] The shorter T_2'(^{27}Al) values measured here, even in the absence of radicals (*cf.* ~5 ms), demonstrates that the presence of paramagnets (biradicals) is not the dominating factor of the T_2'(^{27}Al) decay. Here, the short T_2'(^{27}Al) is due to relaxation induced by the motional modulation of the quadrupolar interaction, which is not present in the case of the ^{13}C nucleus of urea. The slowing of surface motion between RT and 104 K accounts then for the increase in T_2'(^{27}Al). The fact that the T_2'(^{27}Al) barely changes upon the addition of solvents shows that any interaction between the solvent and the surface does not induce modifications in the local motions of the surface. The decrease of T_2' of the surface ^{27}Al nuclei with increasing biradical concentration for the case of γ-alumina impregnated with bTbK in TBE shows that, although it is not the dominating factor, the biradical concentration does have an effect here. This suggests that bTbK is, on average, closer to the surface (possibly physisorbed on the γ-alumina) than TOTAPOL. This claim is further substantiated by analyzing the 'bleaching' of the sample upon the addition of the polarizing agent. Here, bleaching refers to an observed loss of NMR signal intensity resulting from the presence of the paramagnets, in the absence of μw irradiation. 50 % surface signal loss (from a CT-CP experiment) is noted for γ-alumina upon adding ~6 mM of bTbK in TBE, whereas ~10 mM of TOTAPOL in [$^2H_6$]DMSO/^2H_2O/H_2O is required to obtain the same signal losses at the surface of the material. The bleaching of the sample is one reason that the ASR, rather than ε_{DNP}, should be taken into account when discerning the relevance of DNP. Additionally, ε_{DNP} measured via $^1H \rightarrow ^{13}C$ CP (the ^{13}C nuclei are in the solvents) is equal to that measured for surface ^{27}Al via $^1H \rightarrow ^{27}Al$ CT-CP for the system doped with TOTAPOL, whereas for the system doped with bTbK the ε_{DNP} for $^1H \rightarrow ^{13}C$ CP was less than that of surface ^{27}Al (ε_{DNP} = 14, compared to 22, data not shown). This

again suggests that there is a non-uniform distribution of bTbK in the solvent, with a majority close to the surface of the γ-alumina particles. Moreover, the similarity of ε_{DNP} for both $^{1}H \rightarrow ^{13}C$ CP and $^{1}H \rightarrow ^{27}Al$ CT-CP for the system doped with TOTAPOL, suggests that there are negligible buried ^{1}Hs (i.e. hydroxyl groups) in the bulk of the γ-alumina. If there were buried ^{1}Hs that could contribute significantly to ^{27}Al CP then a lower ε_{DNP} than seen for $^{1}H \rightarrow ^{13}C$ CP would result since these bulk ^{1}Hs would be hyperpolarized to a lesser extent than surface (and solvent) ^{1}Hs due to a further average distance from the TOTAPOL (assuming insignificant spin diffusion), as has been shown for silica nanoparticles that do contain some bulk hydroxyls.[48] This is consistent with previous NMR studies that have already demonstrated that most protons in γ-alumina are located near the surface.[6,49]

The time constant describing the time required for the nuclear polarization to reach an equilibrium state from zero, labeled T_B here, is another important factor since this usually determines the recycle delay, i.e. the delay between consecutive NMR acquisitions. Therefore, it has a direct consequence on the ASR. The variation of T_B for ^{1}H (T_B^{1H}), measured indirectly with a saturation recovery experiment using a CT-CP step, as a function of biradical concentration is given in Fig. 2 (b). T_B^{1H} follows almost exactly the same trend as T_D^{CP}, i.e. T_B^{1H} values decrease for increasing concentration of radicals and are always higher for samples impregnated with TOTAPOL in $[^{2}H_6]DMSO/^{2}H_2O/H_2O$ than for those impregnated with bTbk in TBE. The CT-CP step allows for the measurement of T_B^{1H} of the protons in direct proximity to the surface but owing to a coupled proton network, T_B^{1H} of surface protons can be related to T_B^{1H} of the protons in the bulk solvent. Even in the absence of radicals, T_B^{1H} of protons in $[^{2}H_6]DMSO/^{2}H_2O/H_2O$ is much longer than the T_B^{1H} of protons in TBE, as shown in Fig. 2 (c). Although a reduced T_B^{1H} permits an increased optimal rate of experimental signal averaging, the increased concentrations

of polarizing agents required to achieve this reduction can also induce detrimental effects such as signal bleaching and a shortening of T_D^{CP} and $T_2'(^{27}Al)$ times (*vide supra*). Therefore, a favorable compromise should be attained.

This favorable compromise can be found through the ASR since it takes into account all the benefits as well as the detrimental aspects of a certain experiment. For a $^{1}H \rightarrow ^{27}Al$ CT-CP experiment on γ-alumina, the ASR is detailed in Fig. 2 (b). The ASR is scaled, as defined, with respect to pure γ-alumina, recorded at RT. It is evident that MAS-DNP of γ-alumina impregnated with 5 mM bTbK in TBE returns the highest ASR: 9.5. This corresponds to an experimental time-saving factor of ~90, compared to a conventional RT experiment. It should be highlighted that the ASR of pure γ-alumina at 104 K is 6.8: 3.6 from increased thermal polarization and decreased thermal noise[33] and the remaining factor of 1.9 possibly coming from improved CP conditions at low temperature.[17] Therefore, it is more worthwhile to record a $^{1}H \rightarrow ^{27}Al$ CT-CP spectrum of pure γ-alumina at 104 K than it is to record a DNP-enhanced spectrum for almost all the sample preparations attempted. However, it should also be noted that TOTAPOL and bTbK are now not the current benchmarks in terms of ε_{DNP} and other, more efficient biradicals (e.g. AMUPOL[50] and TEKPOL[51]) could give larger ASRs. The reason for the small ASR values is the signal averaging. The experimental repetition delay required for maximum sensitivity for the pure γ-alumina sample, both at RT and 104 K was less than 200 ms for $^{1}H \rightarrow ^{27}Al$ CT-CP, whereas for the γ-alumina impregnated with 5 mM TOTAPOL in $[^{2}H_6]DMSO/^{2}H_2O/H_2O$ at 104 K it was ~19 s for the same experiment. This means that one can repeat an experiment more than 100 times on the pure γ-alumina sample in the time it takes to record one experiment on the γ-alumina impregnated with 5 mM TOTAPOL in $[^{2}H_6]DMSO/^{2}H_2O/H_2O$. For the sample studied here, the larger T_B^{1H} value then dramatically reduces the efficacy of performing DNP.

Nevertheless, all tested samples show an ASR > 1, except for the samples containing 0 mM of biradicals. Therefore, performing MAS-DNP in the manner detailed herein is useful and results in experimental time-savings compared to conventional RT experiments. Even so, a point can be made for simply performing low temperature NMR (~100 K), without the need for exogenous biradicals and μw irradiation, on the pure sample studied here as this also returns good time-savings (factor of ~50).

The similarity in the trends shown above for T_B^{1H} and T_D^{CP} results from the involvement of protons. In contrast, $T_2'(^{27}Al)$ is measured for the surface ^{27}Al nuclei under high power heteronuclear ^1H decoupling, so there will be no influence coming from the protons. In fact, ~80 kHz of SPINAL-64[52] decoupling was sufficient to remove the ^1H influence from the measured T_2' (data not shown) and 100 kHz was employed herein. As stated above, the $T_2'(^{27}Al)$ value is dominated by the fluctuation of the quadrupolar interaction. For the case of γ-alumina impregnated with bTbK in TBE, there is also an influence on the $T_2'(^{27}Al)$ of the surface ^{27}Al nuclei coming from a direct interaction with the radicals. Unlike for surface ^{27}Al nuclei studied under decoupling, intrinsic surface ^1H nuclei (in hydroxyls or physisorbed/coordinated water) will be coupled to other ^1H nuclei from the added solvent. Therefore, the addition of solvent will have an effect on measurements that involve protons, as has been shown for T_B^{1H} and T_D^{CP}. Furthermore, unpaired electrons of biradicals dissolved in these solvents will have a larger coupling to solvent protons, compared to surface ^{27}Al nuclei, due to the closer average inter-spin distance and the larger gyromagnetic ratio of the proton. This larger coupling will lead to faster relaxation of the solvent protons, which is then relayed to the surface protons through the dipolar-coupled network, resulting in dramatically shorter T_B^{1H} and T_D^{CP} times for surface protons as the concentration of biradicals increases.

The biradical bTbK can be dissolved in a DMSO/water mixture as long as the DMSO proportion is high, such as the 78 % (weight) used here. This allows for a direct comparison between the TOTAPOL and bTbK biradicals. For γ-alumina impregnated with 20 mM bTbK in [$^2H_6$]DMSO/^2H_2O/H_2O the DNP enhancement for $^1H \rightarrow ^{27}Al$ CT-CP, $\varepsilon_{DNP,} = 26$ (*cf.* $\varepsilon_{DNP} = 22$ for 20 mM TOTAPOL). However, the T_B^{1H} of surface protons was ~20 s (*cf.* ~4 s for 20 mM TOTAPOL). This data can be found in the Supporting Information (Fig. S2). This significant difference in the observed T_B^{1H} between the sample preparations with TOTAPOL and bTbK is highly interesting since it could suggest that the radicals affect the glassing properties differently or that there is a difference in the electronic relaxation properties between the two, but this will not be investigated further here. Nevertheless, the relatively long T_B^{1H} measured for the sample with bTbK in [$^2H_6$]DMSO/^2H_2O/H_2O does show that it is not a good choice of sample preparation for γ-alumina, with respect to an ASR.

Henceforth, further sample analysis will be performed using DNP-enhanced SSNMR of γ-alumina impregnated with 5 mM bTbK in TBE, since this showed the best ASR. This sample preparation was the optimum compromise between experimental recycle delay, sample bleaching, DNP enhancement, longer-lived coherences (T_D^{CP} and $T_2'(^{27}Al)$), and various other factors.

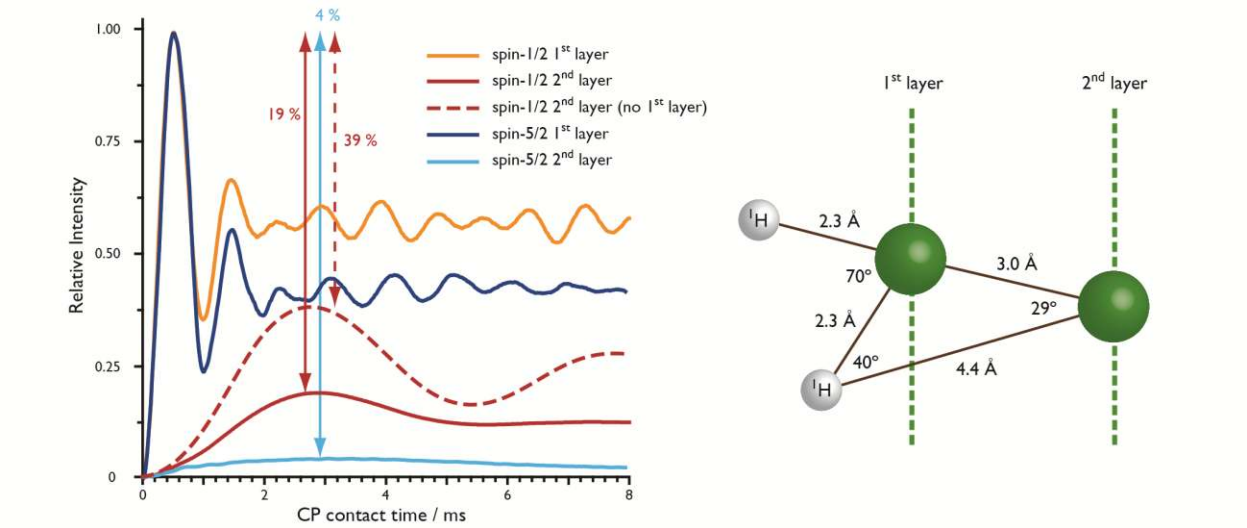

Figure 3. SPINEVOLUTION[53] simulations of the $^{1}H \rightarrow X$ CP efficiency as a function of CP contact time for the 4-spin system shown on the right (replicating an alumina or silica surface). For both the X = spin-1/2 case and the X = spin-5/2 case the external magnetic field was 9.4 T and the corresponding X Larmor frequency was 104 MHz, the MAS rate was 8 kHz and a square n = 1 CP matching condition was used with a ^{1}H RF field of 18 kHz. For the X = spin-5/2 case the quadrupolar coupling constant, C_Q, was 3 MHz and the asymmetry parameter of the electric field gradient tensor, $\eta_{||}$, was 0.25. Chemical shift anisotropy and *J*-coupling were not included in the simulations but all dipolar interactions were included.

One of the underlying questions of the recent surge of DNP-enhanced surface studies is that of what ones means by 'surface'. To that extent, simulations of CP penetration depths were performed using the SPINEVOLUTION[53] program and the model surface system illustrated in Fig. 3. The model was chosen to represent the hydroxylated surface of an oxide (Al_2O_3 or SiO_2), since this type of material has received extensive recent attention for DNP-enhanced SSNMR studies[3,34,38,39,48,54] and is of relevance for the study herein. It can be seen from the CP dynamics (Fig. 3, left) that there is a substantial difference in transferable polarization to the second layer

when the system contains two spin-5/2 nuclei compared to a system containing two spin-1/2 nuclei. For a CP contact time of 4 ms, which maximizes the polarization transfer to the second-layer nuclei, only 4 % of the polarization compared to the first layer is achieved for the second layer for the quadrupolar case, whereas for the spin-1/2 case this value is 19 %. ^{27}Al nuclei are 100 % isotopically abundant, naturally. However, ^{29}Si nuclei are only ~4.7 % naturally abundant. This means that, statistically, a second (or 3rd or 4th) layer ^{29}Si nucleus will not experience a ^{29}Si nucleus in between itself and the ^{1}H nuclei. If the first layer nucleus is given spin-0 and the second layer spin-1/2 then the second layer can achieve a relative polarization of 39 % at a contact time of 2.9 ms. To more correctly reproduce the ^{29}Si case, the gyromagnetic ratio was changed from that of ^{27}Al to that of ^{29}Si (i.e. by a factor of 0.76) and this then gave a maximum value of 28 % attainable polarization at the second layer and a slightly longer optimal CP contact time of 3.2 ms. To go further with this analysis, signal decay during the CP should be taken into account. The experimentally observed decay constant during CP (T_D^{CP}), for the sample used to obtain Fig. 1 (a), was 2.4 ms (see Fig. 2(a)). Compare this to the same decay constant for ^{1}H$\rightarrow^{29}$Si CP, which can be on the order of many tens of ms.[55] Including this signal decay into the analysis, for the spin-5/2 case, the second layer could have a maximum of only 2 % of the polarization compared to the first layer. The simulated optimum CP contact time for transfer to the first layer when including this relaxation is ~ 0.5 ms. The experimentally measured optimum CP contact time is 0.55 ms (see Fig. S3). The good agreement validates the simulations and demonstrates that, experimentally, ^{1}H$\rightarrow^{27}$Al CP for γ-alumina (in the reduced surface proton mobility regime at ~100 K)[17] can be used to polarize only the first surface layer, since any polarization transferred to the second or deeper layers will be negligible. Consequently, for specific systems, CP can be used for '*primostrato*' NMR.

It should be pointed out that the CP dynamics depend upon the size of the quadrupolar interaction for each nucleus. For large C_Q values, spin-locking and uniform excitation of the CT are less efficient and the CP efficiency decreases accordingly. It could be envisaged that the first layer has a much larger quadrupolar coupling constant, C_Q, than the second layer. For example, simulations (not shown) predict that for a first layer nucleus with C_Q = 10 MHz and a second layer nucleus with a C_Q = 3 MHz, the second layer would be able to at-tain a relatively significant polarization so that it would be observable (32 % at ~ 0.5 ms CP contact time). Moreover, allowing for a longer CP contact time (3.3 ms) would result in greater (4 times) transfer efficiency to the second layer compared to the first. Nonetheless, as can be seen in Fig. 3, the second layer would require a relatively long time to build up this polarization and, assuming T_D^{CP} was long enough to permit its observation, this would be evident in CP build-up experiments since the optimum $^1H \rightarrow ^{27}Al$ CP transfer would be observed at longer contact times. Such an observation was not made for any of the γ-alumina samples studied here, including those impregnated with TOTAPOL or bTbk solutions (see Fig. S3).

Reverting to the ^{29}Si case, $^1H \rightarrow ^{29}Si$ CP does *not* constitute *primostrato* NMR for all CP contact times since polarization can be transferred to a multitude of layers and determining the cutoff is not straightforward. However, it is accepted that CP is generally only effective over < 1 nm,[56] which, for silica (SiO_2), gives the cutoff at about the 4th layer. This large penetration depth is fairly well known since bulk ^{29}Si resonances in silica can have very long CP buildup times as magnetization travels further inwards from the surface.[55]

Selectivity of the first surface layer is highly desired because chemical properties are usually related to this layer and this is especially true in the case of catalysts. However, it is also

often desirable to be able to exclude the surface and only study the bulk. In a similar way that the surface protons can be used to select the surface, they can also be used to eliminate signals from the surface. Dipolar couplings of surface nuclei to protons, which were previously used to mediate CP, can also be used to dephase these surface nuclei. This is the basis for the '*bulk-filtered*' experiment presented here. Fig. 4 (a) shows the pulse sequence used to calibrate the bulk-filter, which is contained within and given explicitly in Fig. S4. During the bulk-filter, continuous wave irradiation is applied on the ^{1}H channel with a power that will interfere with the MAS rate ($\omega_r/(2\pi)$) such that the heteronuclear dipolar coupling is reintroduced. For the heteronucleus, ^{27}Al here, a simple spin-echo block is used during this recoupling period. ^{27}Al nuclei with a coupling to ^{1}H nuclei will be dephased during this period whereas those without this coupling will be refocused, i.e. the signals from the surface will be removed, but those from the bulk will remain. Once calibrated, this 'bulk-filter' sequence can be easily added to existing experiments so that these experiments become sensitive to only bulk material. It is worth noting that the 'bulk-filter' is not only applicable to protonated surfaces, but also to many systems where the removal of signals from nuclei with couplings to specific other nuclei may be required.

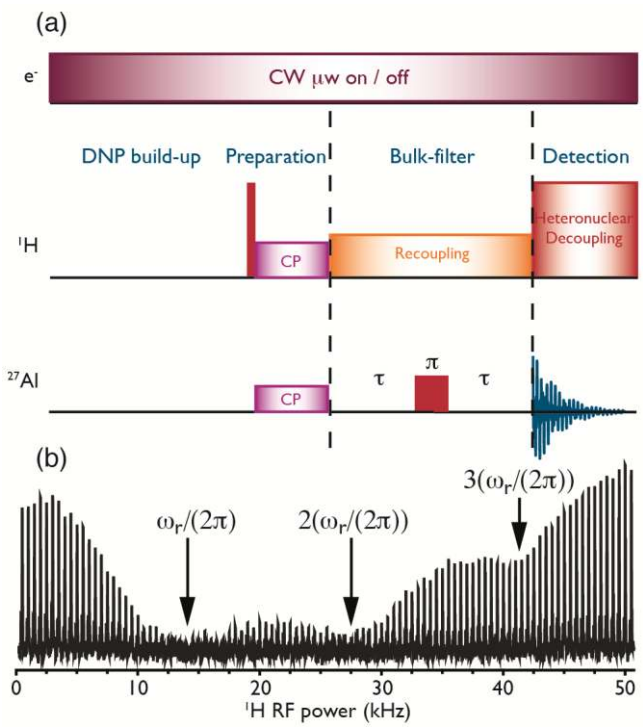

Figure 4. The bulk-filter experiment. (a) The pulse sequence used to calibrate a bulk-filter block, which is shown as a stand-alone sequence between the dashed lines. (b) The recoupling power is varied using an arbitrary time for the bulk-filter block (~4 ms here) until an efficient condition (equal to the MAS rate, $\omega_r/(2\pi)$) is found where the returned signal is minimal. Then, using this calibrated recoupling power, the time period, τ, is increased in integer multiples of the rotor period starting from 1. Here, we used the smallest τ value, for which the returned signal is < 10 % of the signal of the first point.

It has been inferred that the penta-coordinated Al^V site resides primarily on the surface of γ-alumina.[20] With *primostrato* and *bulk-filtered* NMR it should be possible to definitively characterize the whereabouts of this catalytically important site. However, at the magnetic field strengths used here (9.4 T) there is not enough spectral resolution to be able to distinguish the Al^V site. Even at magnetic field strengths of ~19 T, this site remains as only a 'bump' in the

spectrum.[20] Nonetheless, elegant experiments have been devised that can dramatically improve the resolution of spectra of quadrupolar nuclei. One such experiment, the Multiple Quantum Magic Angle Spinning (MQMAS) experiment,[24,25] uses a clever combination of RF pulses, multi-dimensional NMR and processing to obtain a spectral dimension free of the second-order quadrupolar broadening, which cannot be removed with MAS alone. Furthermore, the multi-dimensional nature of this experiment produces a greater separation between peaks.

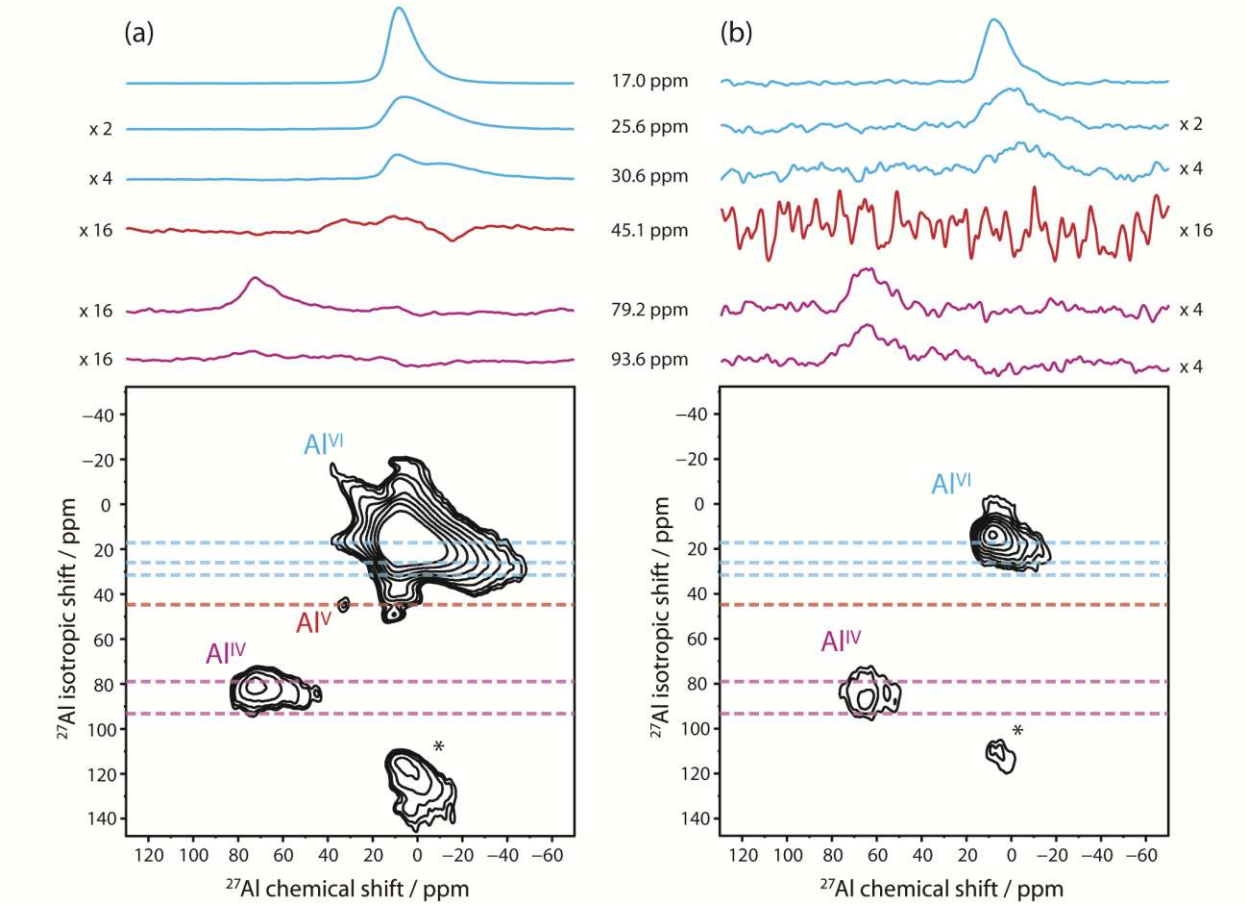

Figure 5. Sheared MQMAS spectra for γ-alumina impregnated with 5 mM bTbK in TBE: (a) DNP-enhanced *primostrato*-3QMAS and (b) *bulk-filtered*-3QMAS, both recorded with a MAS rate of ~14 kHz and a sample temperature of ~104 K. The total acquisition time was ~7 hours for each. The contour levels used in (a) and (b) are not the same. Also shown (top) are horizontal

cross-sections taken at the indicated isotropic shift values with indicated intensity multiplications used for improved viewing. Asterisks denote spinning sidebands.

Primostrato z-filtered MQMAS experiments could be recorded by using an initial DNP-enhanced $^{1}H \rightarrow ^{27}Al$ CP step to excite the required multiple-quantum coherences (in this case triple-quantum, 3Q).[57] A resulting spectrum for the γ-alumina is given in Fig. 5 (a). Additionally, 3QMAS data concerning only the bulk of this material could be recorded by adding a 'bulk-filter' block to a standard z-filtered MQMAS experiment. The corresponding spectrum resulting from this experiment is shown in Fig. 5 (b). The pulse sequences used to acquire these spectra can be found in Fig. S5. Note that both spectra have been processed using a shearing transformation, as is common practice for MQMAS data, so that the horizontal dimension displays the purely isotropic data. Notably, it is evident that a peak relating to penta-coordinated Al^{3+} is only present in the *primostrato* spectrum (Fig. 5 (a)).

Cross-sections from the MQMAS spectra are also given in Fig. 5 and further highlight the observation of the Al^{V} site only in the *primostrato* spectrum. Additionally, these cross-sections (and the 1D *primostrato* and *bulk-filtered* experiments given in Fig. S1(c)) show that the ratio of Al^{VI} to Al^{IV} sites is much greater in the first surface layer compared to the bulk. This indicates the existence of a surface reconstruction with an excess of Al^{3+} in octahedral sites, as has been recently suggested.[8] The cross-section for the Al^{V} site allows a fitting of the data and approximate NMR parameters to be extracted for this surface moiety. Fig. 6 shows fits for various ^{27}Al sites extracted from the cross-sections in Fig. 5 and the corresponding isotropic chemical shifts (δ(iso)), C_Q and η_Q parameters. The C_Q of 7.0 ± 0.3 MHz extracted for Al^{V} is consistent with that obtained from theoretical surface models containing this particular site.[22]

However, it should be pointed out that the cross-section for the Al^{V} site could be perturbed by a contribution coming from Al^{VI} at < 20 ppm. In this case, the values of C_Q and η_Q for Al^{V} would be different. Discrete resonances were taken for the fits and demonstrate that there is a distribution of NMR parameters observed for Al^{IV} and Al^{VI} coordination states, both on the surface and in the bulk, in agreement with what has previously been shown for γ-alumina.[58] This spread of parameters can also be modelled by a Czjzek distribution.[59] Furthermore, although the *bulk-filtered* MQMAS experiment shows certain bulk Al^{IV} sites with a relatively large C_Q (7.5 ± 0.3 MHz), consistent with the literature,[7] these sites are almost unobservable with the *primostrato* version. This indicates that the geometrical symmetry of the tetrahedral Al^{IV} surface moieties is greater than those in the bulk, which could be counter intuitive for a crystalline material. Nevertheless, surface reconstruction could lead to an ordered surface and a disordered sub-surface.[8] Indeed, the crystalline core of the γ-alumina nanoparticles used here is expected to be only ~ 1/3 of the particle size.[8] This leaves a majority of disordered sub-surface, which can explain the distribution of NMR parameters taken from the *bulk-filtered* MQMAS experiment. It should be noted that at the static magnetic field strength used here (~10 T) any ^{27}Al resonances with a relatively high C_Q (i.e. > 10 MHz) will be more difficult to detect due to substantial signal broadening caused by the second order quadrupolar interaction, with some sites possibly being 'invisible'.[7] Higher magnetic field strengths can alleviate this problem to some extent since this interaction is inversely proportional to field strength. However, MAS-DNP at higher static magnetic field strengths can be less efficient[27] and corresponding acquisition of *primostrato* MQMAS data will be more challenging.

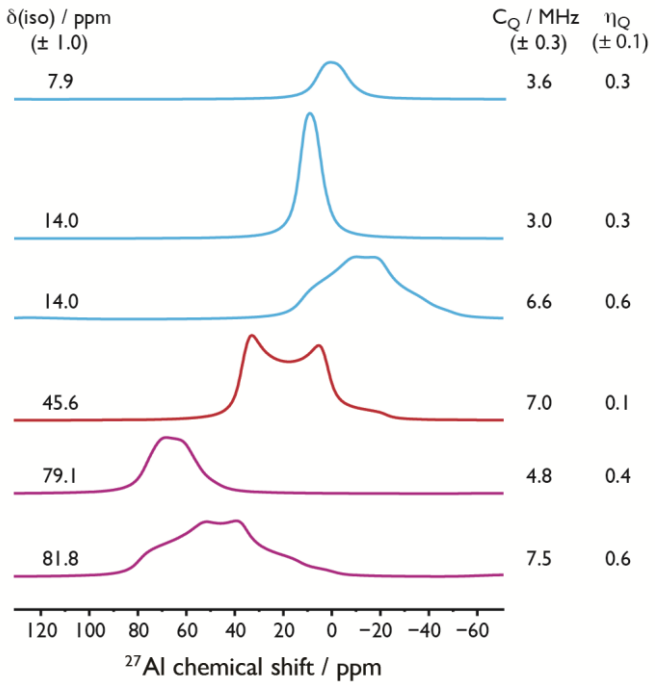

Figure 6. Fits to quadrupolar lineshapes of contributing resonances to the cross-sections from MQMAS data shown in Fig. 5 (a) and (b). The δ(iso), quadrupolar coupling constants (C_Q) and quadrupolar asymmetry parameters ($\eta_{||}$) used for the fits are given in the figure. Al^{VI}, Al^{V}, and Al^{IV} sites are represented by blue, red, and purple, respectively.

As a comparison to the *bulk-filtered* MQMAS experiment, which does not return a good signal-to-noise ratio, a standard MQMAS experiment was also performed (Fig. S6). They both return similar results although the sensitivity of the standard MQMAS experiment is much better. Owing to the smaller amount of surface relative to bulk, signal coming from the surface will be of lower intensity for the standard MQMAS experiment, so the similarity is expected. Nevertheless, the *bulk-filtered* experiment was used to be sure that there was no signal present from the first layer of the material. Moreover, the standard MQMAS experiment was recorded because the Al^{V} sites could be potentially located in the bulk as hydroxylated defects, which

would be unobservable in the *bulk-filtered* experiment. Since the sensitivity of the standard MQMAS is much greater than the *bulk-filtered* equivalent, and no Al^{V} sites are observed in either, it can be concluded that the vast majority of (if not all) penta-coordinated Al^{3+} is found in the first surface layer of hydrated γ-alumina.

To examine the literature suggestion[34] that the aqueous sample preparation and/or the TOTAPOL biradical can coordinate to, and thus obscure, the penta-coordinated Al^{3+} site, the same experiment to that of Fig. 5 (a) was performed but using this alternative, aqueous preparation method. The resulting spectrum (Fig. S7) is almost identical to that of Fig. 5 (a). Therefore, neither the solvent mixture nor the TOTAPOL biradical coordinate sufficiently (if at all) to remove the presence of this Al^{V} site. The downside of the aqueous sample preparation is the smaller ASR that necessitates longer experimental times.

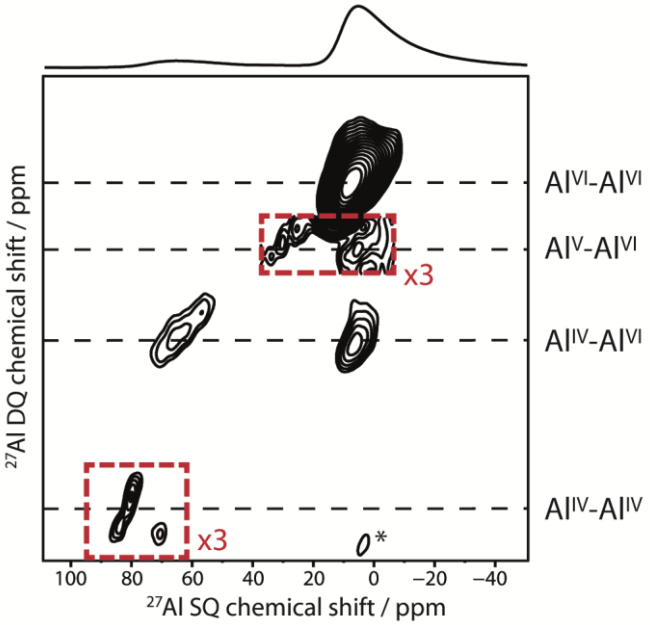

Figure 7. DNP-enhanced surface-selective DQ-SQ ^{27}Al homonuclear dipolar correlation spectrum of γ-alumina impregnated with 5 mM TOTAPOL in $[^{2}H_6]DMSO/^{2}H_2O/H_2O$, recorded

using a MAS rate of ~14 kHz and a sample temperature of ~104 K. The total acquisition time was ~6 hours. Also shown (top) is the $^{1}H \rightarrow ^{27}Al$ CT-CP spectrum, recorded under the same conditions. Asterisks denote spinning sidebands.

To gain additional structural information concerning the location of the Al^{V} site on the surface, ^{27}Al homonuclear correlation spectra were recorded. We have recently shown that these experiments are now readily accessible with the application of DNP.[54] Like previously,[54] we use the $BR2_2^1$ symmetry-based recoupling sequence to excite double quantum coherences between dipolar-coupled ^{27}Al spin pairs. After an initial DNP-enhanced *primostrato* $^{1}H \rightarrow ^{27}Al$ CT-CP step, the hyperpolarized ^{27}Al spins are recoupled using the $BR2_2^1$ sequence and only these coupled spins are selected by the experiment. Therefore, the resulting spectrum, shown in Fig. 7 for the sample of γ-alumina studied here, indicates the spatial proximities between ^{27}Al sites. This spectrum was acquired in only 6 h. Note that Fig. 7 does not show *primostrato* NMR because the recoupling of *primostrato* ^{27}Al nuclei could be to other ^{27}Al nuclei that reside in deeper layers (although further than the second layer nuclei is unlikely). For *primostrato* recoupling the TSAR methodology[60] should be employed as this utilizes couplings to ^{1}H nuclei for the transfer and will thus be limited to the first surface layer. This will hopefully be demonstrated in a future study. Furthermore, the spectrum in Fig. 7 was recorded using the sample of γ-alumina impregnated with 5 mM TOTAPOL in $[^{2}H_6]DMSO/^{2}H_2O/H_2O$. Owing to the signal decay during the application of the $BR2_2^1$ sequence, the longer coherence lifetimes noted for the γ-alumina impregnated with 5 mM TOTAPOL in $[^{2}H_6]DMSO/^{2}H_2O/H_2O$ render this sample preparation just as practical for this particular homonuclear correlation experiment, in terms of resulting ASR, as the γ-alumina impregnated with 5 mM bTbK in TBE, and significantly more favorable than a similar conventional room temperature experiment.

Fig. 7 shows Al^{VI}–Al^{VI}, Al^{V}–Al^{VI}, Al^{IV}–Al^{VI}, and Al^{IV}–Al^{IV} correlations. Al^{IV}–Al^{V} and Al^{V}–Al^{V} correlations are absent from Fig. 7 but these could be below the observable signal threshold since they are between the least abundant sites. Close proximities of surface Al^{IV} and Al^{V} sites could be expected as this has been seen in a related mesoporous alumina material[54] and is presumed from theoretical studies.[13] The proximity of surface Al^{V} sites with other Al^{V} sites is of high interest but improvements to the sensitivity of the experiments shown herein are required before further information in this direction is attainable. Nevertheless, this should be anticipated in the near future due to the continual advancements of DNP methodology and practice.

4. CONCLUSIONS

A detailed comparison between aqueous and hydrophobic sample preparation protocols for low temperature (~104 K) MAS-DNP studies of hydrated γ-alumina nanoparticles was performed. It was shown that although neither preparation perturbed the resulting spectra, the aqueous sample preparation resulted in longer-lived coherences during $^{1}H \rightarrow {}^{27}Al$ CT-CP experiments and also longer ^{1}H polarization build-up times relative to the hydrophobic sample preparation and also to the pure sample without added solvent. Although longer-lived coherences are experimentally advantageous, the longer ^{1}H polarization build-up means that signal-averaging requires more time in between successive accumulations and thus overall sensitivity is impacted. The T_2' of surface ^{27}Al nuclei showed negligible dependence on the addition of solvent but it increased with a decrease in the temperature. This T_2' is thus dominated by motionally-induced local fluctuations of the quadrupolar interaction, which are reduced as the temperature decreases. Nevertheless, the addition of bTbK to the hydrophobic solvent and γ-alumina has the effect of reducing the T_2' of surface ^{27}Al nuclei, unlike for TOTAPOL in an

aqueous mixture with γ-alumina. This is because bTbK is closer, on average, to the surface of the γ-alumina, likely due to a surface affinity. This proximity facilitated direct MAS-DNP of ^{27}Al nuclei and also aided the return of the best absolute sensitivity for ^{1}H→^{27}Al CT-CP experiments when using only 5 mM of the biradical.

Simulations showed that these low temperature ^{1}H→^{27}Al CT-CP experiments can be considered as *primostrato* NMR experiments for γ-alumina since ^{27}Al nuclei only in the first surface layer can receive significant polarization from surface protons, after experimental demonstration that there are no detectable protons (hydroxyl groups) in the bulk. A new experiment was described that can also be used to selectively probe a sample by reducing signals stemming from nuclei with a common coupling to a heteronucleus. For the case of γ-alumina this experiment was used as a *bulk-filter*, whereby surface ^{27}Al signals could be 'removed' owing to the common coupling to ^{1}H nuclei. The *primostrato* and *bulk-filter* experiments were combined with the MQMAS experiment to add selectivity to this high-resolution technique. Notably, it was then shown that penta-coordinated Al^{3+} ions can only be located in the first surface layer of hydrated γ-alumina. Selective ^{27}Al homonuclear correlation experiments were also performed to attempt to gain further information on the surface structure. They showed that Al^{V} sites are located as neighbors to Al^{VI} sites. However, the small amount of Al^{V} present necessitates further improvements in sensitivity before other associated correlations or lack thereof can be considered conclusive.

ASSOCIATED CONTENT

Supporting Information. Further experimental details, additional 1D and 2D (MQMAS) NMR spectra, NMR pulse sequences for the bulk-filter, *bulk-filtered* MQMAS, and DNP-enhanced *primostrato* MQMAS experiments, as well as steady-state polarization and cross-polarization build up curves are given. This material is available free of charge via the Internet at http://pubs.acs.org.

AUTHOR INFORMATION

Corresponding Author

* gael.depaepe@cea.fr

Author Contributions

The manuscript was written through contributions of all authors. All authors have given approval to the final version of the manuscript.

ACKNOWLEDGMENT

This work was supported by the French National Research Agency through the Labex ARCANE (ANR-11-LABX-0003-01) and the "programme blanc" (ANR-12-BS08-0016-01). The RTB is acknowledged for financial support. T. N. D. acknowledges CEA and CNRS for his PhD fellowship.

REFERENCES

(1) McGuire, G. E.; Fuchs, J.; Han, P.; Kushmerick, J. G.; Weiss, P. S.; Simko, S. J.; Nemanich, R. J.; Chopra, D. R. Surface Characterization. *Anal. Chem.* **1999**, *71*, 373–388.

(2) Becerra, L. R.; Gerfen, G. J.; Temkin, R. J.; Singel, D. J.; Griffin, R. G. Dynamic Nuclear Polarization with a Cyclotron Resonance Maser at 5 T. *Phys. Rev. Lett.* **1993**, *71*, 3561–3564.

(3) Rossini, A. J.; Zagdoun, A.; Lelli, M.; Lesage, A.; Copéret, C.; Emsley, L. Dynamic Nuclear Polarization Surface Enhanced NMR Spectroscopy. *Acc. Chem. Res.* **2013**, *46*, 1942–1951.

(4) Hartmann, S.; Hahn, E. Nuclear Double Resonance in the Rotating Frame. *Phys. Rev.* **1962**, *128*, 2042–2053.

(5) Maciel, G. E.; Sindorf, D. W. Silicon-29 NMR Study of the Surface of Silica Gel by Cross Polarization and Magic-Angle Spinning. *J. Am. Chem. Soc.* **1980**, *102*, 7606–7607.

(6) Morris, H. D.; Ellis, P. D. Aluminum-27 Cross Polarization of Aluminas. The NMR Spectroscopy of Surface Aluminum Atoms. *J. Am. Chem. Soc.* **1989**, *111*, 6045–6049.

(7) Wischert, R.; Florian, P.; Copéret, C.; Massiot, D.; Sautet, P. Visibility of Al Surface Sites of γ-Alumina: A Combined Computational and Experimental Point of View. *J. Phys. Chem. C* **2014**, *118*, 15292–15299.

(8) Rozita, Y.; Brydson, R.; Comyn, T. P.; Scott, A. J.; Hammond, C.; Brown, A.; Chauruka, S.; Hassanpour, A.; Young, N. P.; Kirkland, A. I.; et al. A Study of Commercial Nanoparticulate γ-Al_2O_3 Catalyst Supports. *ChemCatChem* **2013**, *5*, 2695–2706.

(9) Trueba, M.; Trasatti, S. P. γ-Alumina as a Support for Catalysts: A Review of Fundamental Aspects. *Eur. J. Inorg. Chem.* **2005**, *2005*, 3393–3403.

(10) Hudson, L. K.; Misra, C.; Perrotta, A. J.; Wefers, K.; Williams, F. S. Aluminum Oxide. In *Ullmann's Encyclopedia of Industrial Chemistry*; Pelc, H., Ed.; Wiley-VCH: Weinheim, Germany, 2000; pp. 607–645.

(11) Joubert, J.; Salameh, A.; Krakoviack, V.; Delbecq, F.; Sautet, P.; Copéret, C.; Basset, J. M. Heterolytic Splitting of H_2 and CH_4 on γ-Alumina as a Structural Probe for Defect Sites. *J. Phys. Chem. B* **2006**, *110*, 23944–23950.

(12) Salameh, A.; Copéret, C.; Basset, J.-M.; Böhm, V. P. W.; Röper, M. Rhenium(VII) Oxide/Aluminum Oxide: More Experimental Evidence for an Oxametallacyclobutane Intermediate and a Pseudo-Wittig Initiation Step in Olefin Metathesis. *Adv. Synth. Catal.* **2007**, *349*, 238–242.

(13) Digne, M.; Sautet, P.; Raybaud, P.; Euzen, P.; Toulhoat, H. Use of DFT to Achieve a Rational Understanding of Acid-Basic Properties of γ-Alumina Surfaces. *J. Catal.* **2004**, *226*, 54–68.

(14) Paglia, G.; Rohl, A.; Buckley, C.; Gale, J. Determination of the Structure of γ-Alumina from Interatomic Potential and First-Principles Calculations: The Requirement of Significant Numbers of Nonspinel Positions to Achieve an Accurate Structural Model. *Phys. Rev. B* **2005**, *71*, 224115.

(15) Ferreira, A. R.; Küçükbenli, E.; Leitão, A. A.; de Gironcoli, S. Ab Initio ^{27}Al NMR Chemical Shifts and Quadrupolar Parameters for Al_2O_3 Phases and Their Precursors. *Phys. Rev. B* **2011**, *84*, 235119.

(16) Knozingert, H.; Ratnasamy, P. I. Catalytic Aluminas: Surface Models and Characterization of Surface Sites. *Catal. Rev. Sci. Eng.* **1978**, *17*, 31–70.

(17) Huggins, B. A.; Ellis, P. D. Aluminum-27 Nuclear Magnetic Resonance Study of Aluminas and Their Surfaces. *J. Am. Chem. Soc.* **1992**, *114*, 2098–2108.

(18) Decanio, E.; Edwards, J. C.; Bruno, J. W. Solid-State ^{1}H MAS NMR Characterization of γ-Alumina and Modified γ-Aluminas. *J. Catal.* **1994**, *148*, 76–83.

(19) Zhang, W.; Sun, M.; Prins, R. Multinuclear MAS NMR Identification of Fluorine Species on the Surface of Fluorinated γ-Alumina. *J. Phys. Chem. B* **2002**, *106*, 11805–11809.

(20) Kwak, J.; Hu, J.; Kim, D.; Szanyi, J.; Peden, C. Penta-Coordinated Al^{3+} Ions as Preferential Nucleation Sites for BaO on γ-Al_2O_3: An Ultra-High-Magnetic Field ^{27}Al MAS NMR Study. *J. Catal.* **2007**, *251*, 189–194.

(21) Delgado, M.; Delbecq, F.; Santini, C. C.; Lefebvre, F.; Norsic, S.; Putaj, P.; Sautet, P.; Basset, J. Evolution of Structure and of Grafting Properties of γ-Alumina with Pretreatment Temperature. *J. Phys. Chem. C* **2012**, *116*, 834–843.

(22) Taoufik, M.; Szeto, K. C.; Merle, N.; Del Rosal, I.; Maron, L.; Trébosc, J.; Tricot, G.; Gauvin, R. M.; Delevoye, L. Heteronuclear NMR Spectroscopy as a Surface-Selective Technique: A Unique Look at the Hydroxyl Groups of γ-Alumina. *Chem. Eur. J.* **2014**, *20*, 4038–4046.

(23) Ferreira, A. R.; Küçükbenli, E.; de Gironcoli, S.; Souza, W. F.; Chiaro, S. S. X.; Konstantinova, E.; Leitão, A. A. Structural Models of Activated γ-Alumina Surfaces Revisited: Thermodynamics, NMR and IR Spectroscopies from Ab Initio Calculations. *Chem. Phys.* **2013**, *423*, 62–72.

(24) Frydman, L.; Harwood, J. S. Isotropic Spectra of Half-Integer Quadrupolar Spins from Bidimensional Magic-Angle Spinning NMR. *J. Am. Chem. Soc.* **1995**, *117*, 5367–5368.

(25) Medek, A.; Harwood, J. S.; Frydman, L. Multiple-Quantum Magic-Angle Spinning NMR: A New Method for the Study of Quadrupolar Nuclei in Solids. *J. Am. Chem. Soc.* **1995**, *117*, 12779–12787.

(26) Zagdoun, A.; Rossini, A. J.; Gajan, D.; Bourdolle, A.; Ouari, O.; Rosay, M.; Maas, W. E.; Tordo, P.; Lelli, M.; Emsley, L.; et al. Non-Aqueous Solvents for DNP Surface Enhanced NMR Spectroscopy. *Chem. Commun.* **2012**, *48*, 654–656.

(27) Song, C.; Hu, K.-N.; Joo, C.-G.; Swager, T. M.; Griffin, R. G. TOTAPOL: A Biradical Polarizing Agent for Dynamic Nuclear Polarization Experiments in Aqueous Media. *J. Am. Chem. Soc.* **2006**, *128*, 11385–11390.

(28) Rosay, M.; Tometich, L.; Pawsey, S.; Bader, R. Solid-State Dynamic Nuclear Polarization at 263 GHz: Spectrometer Design and Experimental Results. *Phys. Chem. Chem. Phys.* **2010**, *12*, 5850–5860.

(29) Mentink-Vigier, F.; Akbey, Ü.; Hovav, Y.; Vega, S.; Oschkinat, H.; Feintuch, A. Fast Passage Dynamic Nuclear Polarization on Rotating Solids. *J. Magn. Reson.* **2012**, *224*, 13–21.

(30) Thurber, K. R.; Tycko, R. Theory for Cross Effect Dynamic Nuclear Polarization under Magic-Angle Spinning in Solid State Nuclear Magnetic Resonance: The Importance of Level Crossings. *J. Chem. Phys.* **2012**, *137*, 084508.

(31) Vega, A. J. CP/MAS of Quadrupolar S=3/2 Nuclei. *Solid State Nucl. Magn. Reson.* **1992**, *1*, 17–32.

(32) Hu, K.-N.; Song, C.; Yu, H.-H.; Swager, T. M.; Griffin, R. G. High-Frequency Dynamic Nuclear Polarization Using Biradicals: A Multifrequency EPR Lineshape Analysis. *J. Chem. Phys.* **2008**, *128*, 052302.

(33) Takahashi, H.; Lee, D.; Dubois, L.; Bardet, M.; Hediger, S.; De Paepe, G. Rapid Natural-Abundance 2D ^{13}C-^{13}C Correlation Spectroscopy Using Dynamic Nuclear Polarization Enhanced Solid-State NMR and Matrix-Free Sample Preparation. *Angew. Chem., Int. Ed.* **2012**, *51*, 11766–11769.

(34) Vitzthum, V.; Miéville, P.; Carnevale, D.; Caporini, M. a; Gajan, D.; Copéret, C.; Lelli, M.; Zagdoun, A.; Rossini, A. J.; Lesage, A.; et al. Dynamic Nuclear Polarization of Quadrupolar Nuclei Using Cross Polarization from Protons: Surface-Enhanced Aluminium-27 NMR. *Chem. Commun.* **2012**, *48*, 1988–1990.

(35) Kasprzyk-Hordern, B. Chemistry of Alumina, Reactions in Aqueous Solution and Its Application in Water Treatment. *Adv. Colloid Interface Sci.* **2004**, *110*, 19–48.

(36) Pagni, R. M.; Kabalka, G. W.; Boothe, R.; Gaetano, K.; Stewart, L. J.; Conaway, R.; Dial, C.; Gray, D.; Larson, S.; Luidhardt, T. Reactions of Unsaturated Compounds with Iodine and Bromine on γ-Alumina. *J. Org. Chem.* **1988**, *53*, 4477–4482.

(37) Joubert, J.; Delbecq, F.; Sautet, P.; Le Roux, E.; Taoufik, M.; Thieuleux, C.; Blanc, F.; Copéret, C.; Thivolle-Cazat, J.; Basset, J.-M. Molecular Understanding of Alumina Supported Single-Site Catalysts by a Combination of Experiment and Theory. *J. Am. Chem. Soc.* **2006**, *128*, 9157–9169.

(38) Lafon, O.; Rosay, M.; Aussenac, F.; Lu, X.; Trébosc, J.; Cristini, O.; Kinowski, C.; Touati, N.; Vezin, H.; Amoureux, J.-P. Beyond the Silica Surface by Direct Silicon-29 Dynamic Nuclear Polarization. *Angew. Chem., Int. Ed.* **2011**, *50*, 8367–8370.

(39) Akbey, Ü.; Altin, B.; Linden, A.; Ozçelik, S.; Gradzielski, M.; Oschkinat, H. Dynamic Nuclear Polarization of Spherical Nanoparticles. *Phys. Chem. Chem. Phys.* **2013**, *15*, 20706–20716.

(40) Blanc, F.; Sperrin, L.; Jefferson, D. A.; Pawsey, S.; Rosay, M.; Grey, C. P. Dynamic Nuclear Polarization Enhanced Natural Abundance ^{17}O Spectroscopy. *J. Am. Chem. Soc.* **2013**, *135*, 2975–2978.

(41) Michaelis, V. K.; Corzilius, B.; Smith, A. A.; Griffin, R. G. Dynamic Nuclear Polarization of ^{17}O: Direct Polarization. *J. Phys. Chem. B* **2013**, *117*, 14894–14906.

(42) Pourpoint, F.; Thankamony, A. S. L.; Volkringer, C.; Loiseau, T.; Trébosc, J.; Aussenac, F.; Carnevale, D.; Bodenhausen, G.; Vezin, H.; Lafon, O.; et al. Probing ^{27}Al-^{13}C Proximities in Metal-Organic Frameworks Using Dynamic Nuclear Polarization Enhanced NMR Spectroscopy. *Chem. Commun.* **2014**, *50*, 933–935.

(43) Rossini, A. J.; Zagdoun, A.; Hegner, F.; Schwarzwälder, M.; Gajan, D.; Copéret, C.; Lesage, A.; Emsley, L. Dynamic Nuclear Polarization NMR Spectroscopy of Microcrystalline Solids. *J. Am. Chem. Soc.* **2012**, *134*, 16899–16908.

(44) Van der Wel, P. C. A.; Hu, K.; Lewandowski, J.; Griffin, R. G. Dynamic Nuclear Polarization of Amyloidogenic Peptide Nanocrystals: GNNQQNY, a Core Segment of the Yeast Prion Protein Sup35p. *J. Am. Chem. Soc.* **2006**, *128*, 10840–10846.

(45) Lafon, O.; Thankamony, A. S. L.; Kobayashi, T.; Carnevale, D.; Vitzthum, V.; Slowing, I. I.; Kandel, K.; Vezin, H.; Amoureux, J.; Bodenhausen, G.; et al. Mesoporous Silica Nanoparticles Loaded with Surfactant: Low Temperature Magic Angle Spinning ^{13}C and ^{29}Si NMR Enhanced by Dynamic Nuclear Polarization. *J. Phys. Chem. C* **2013**, *117*, 1375–1382.

(46) Mehring, M. *Principles of High Resolution NMR in Solids*; Springer Berlin Heidelberg: Berlin, Heidelberg, 1983.

(47) Takahashi, H.; Fernández-de-Alba, C.; Lee, D.; Maurel, V.; Gambarelli, S.; Bardet, M.; Hediger, S.; Barra, A.-L.; De Paëpe, G. Optimization of an Absolute Sensitivity in a Glassy Matrix during DNP-Enhanced Multidimensional Solid-State NMR Experiments. *J. Magn. Reson.* **2014**, *239*, 91–99.

(48) Lee, D.; Monin, G.; Duong, N. T.; Zamanillo Lopez, I.; Bardet, M.; Mareau, V.; Gonon, L.; De Paëpe, G. Untangling the Condensation Network of Organosiloxanes on Nanoparticles Using 2D ^{29}Si-^{29}Si Solid-State NMR Enhanced by Dynamic Nuclear Polarization. *J. Am. Chem. Soc.* **2014**, *136*, 13781–13788.

(49) Pearson, R. M. Wide Line Nuclear Magnetic Resonance Studies on Transition Aluminas - Distribution of Protons between Surface and Bulk Phases. *J. Catal.* **1971**, *23*, 388–394.

(50) Sauvée, C.; Rosay, M.; Casano, G.; Aussenac, F.; Weber, R. T.; Ouari, O.; Tordo, P. Highly Efficient, Water-Soluble Polarizing Agents for Dynamic Nuclear Polarization at High Frequency. *Angew. Chem., Int. Ed.* **2013**, *52*, 10858–10861.

(51) Zagdoun, A.; Casano, G.; Ouari, O.; Schwarzwälder, M.; Rossini, A. J.; Aussenac, F.; Yulikov, M.; Jeschke, G.; Copéret, C.; Lesage, A.; et al. Large Molecular Weight Nitroxide Biradicals Providing Efficient Dynamic Nuclear Polarization at Temperatures up to 200 K. *J. Am. Chem. Soc.* **2013**, *135*, 12790–12797.

(52) Fung, B. M.; Khitrin, A. K.; Ermolaev, K. An Improved Broadband Decoupling Sequence for Liquid Crystals and Solids. *J. Magn. Reson.* **2000**, *142*, 97–101.

(53) Veshtort, M.; Griffin, R. G. SPINEVOLUTION: A Powerful Tool for the Simulation of Solid and Liquid State NMR Experiments. *J. Magn. Reson.* **2006**, *178*, 248–282.

(54) Lee, D.; Takahashi, H.; Thankamony, A. S. L.; Dacquin, J.; Bardet, M.; Lafon, O.; Paëpe, G. De. Enhanced Solid-State NMR Correlation Spectroscopy of Quadrupolar Nuclei Using Dynamic Nuclear Polarization. *J. Am. Chem. Soc.* **2012**, *134*, 18491–18494.

(55) Lee, D.; Balmer, J. A.; Schmid, A.; Tonnar, J.; Armes, S. P.; Titman, J. J. Solid-State Nuclear Magnetic Resonance Studies of Vinyl Polymer/Silica Colloidal Nanocomposite Particles. *Langmuir* **2010**, *26*, 15592–15598.

(56) Protesescu, L.; Rossini, A. J.; Kriegner, D.; Valla, M.; de Kergommeaux, A.; Walter, M.; Kravchyk, K. V; Nachtegaal, M.; Stangl, J.; Malaman, B.; et al. Unraveling the Core-Shell Structure of Ligand-Capped Sn/SnOx Nanoparticles by Surface-Enhanced Nuclear Magnetic Resonance, Mössbauer, and X-Ray Absorption Spectroscopies. *ACS Nano* **2014**, *8*, 2639–2648.

(57) Ashbrook, S. E.; Wimperis, S. Multiple-Quantum Cross-Polarization and Two-Dimensional MQMAS NMR of Quadrupolar Nuclei. *J. Magn. Reson.* **2000**, *147*, 238–249.

(58) Goldbourt, A.; Landau, M. V; Vega, S. Characterization of Aluminum Species in Alumina Multilayer Grafted MCM-41 Using ^{27}Al FAM(II)-MQMAS NMR. *J. Phys. Chem. B* **2003**, *107*, 724–731.

(59) Czjzek, G.; Fink, J.; Götz, F.; Schmidt, H.; Coey, J.; Rebouillat, J.-P.; Liénard, A. Atomic Coordination and the Distribution of Electric Field Gradients in Amorphous Solids. *Phys. Rev. B* **1981**, *23*, 2513–2530.

(60) De Paëpe, G. Dipolar Recoupling in Magic Angle Spinning Solid-State Nuclear Magnetic Resonance. *Annu. Rev. Phys. Chem.* **2012**, *63*, 661–684.

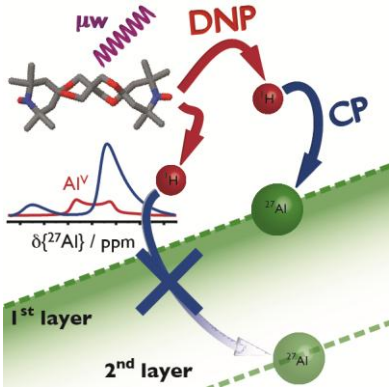

TOC figure